Available online at www.sciencedirect.com
SCIENCE DIRECT®
Journal of Sound and Vibration 290 (2006) 619–639
JOURNAL OF SOUND AND VIBRATION
www.elsevier.com/locate/jsvi

Equivalent rheological and restoring force models for predicting the harmonic response of elastomer specimens

P. Saad[a], A. Al Majid[b], F. Thouverez[a], R. Dufour[b,*]

[a]*Laboratoire de Tribologie et Dynamique des Systèmes, Ecole Centrale de Lyon, UMR CNRS 5513 36, Avenue Guy de Collongue, 69134 Ecully, France*
[b]*Laboratoire de Dynamique des Machines et des Structures, INSA de Lyon, UMR CNRS 5006 18, Bâtiment Jean d'Alembert, 8, Rue des Sciences, 69621 Villeurbanne, France*

Received 5 August 2003; received in revised form 30 November 2004; accepted 11 April 2005
Available online 19 August 2005

Abstract

This article presents two theoretical approaches that simulate the visco-elastic behaviour of elastomer specimens. The first approach, based on an equivalent rheological model, provides a dynamic modulus extracted from a Volterra development of the visco-elastic constitutive law using either relaxation or creep kernels. The second approach establishes a restoring force model based on a first-order differential equation that relates the restoring force to the deflection, the forcing frequency and deflection amplitude dependence being taken into account by the envelope curves of the force–deflection loop.

The two models proposed are first applied to an elastomer cylinder mount made of a small quantity of carbon black filler and then to elastomer plates made of a large quantity of black filler. The cylinder and plates specimens are subjected to traction–compression and shear tests, respectively.

In order to compare the two approaches, the dynamic modulus of the second approach is extracted by applying classical formulae to the force–deflection loop obtained with the restoring force model. Moreover experimental investigations permit comparing the simulated and measured dynamic modulus and validating the two theoretical approaches proposed.

*Corresponding author. Tel.: +33 4 72 43 82 02; fax: +33 4 72 43 89 30.
E-mail address: regis.dufour@insa-lyon.fr (R. Dufour).

0022-460X/$ - see front matter © 2005 Elsevier Ltd. All rights reserved.
doi:10.1016/j.jsv.2005.04.023

1. Introduction

Elastomer specimens are widely used as vibration isolators in particular in automotive applications. Their visco-elastic behaviour is delicate and complicated to model due to nonlinear dependence on pre-load, deflection, temperature and forcing frequency. The modelling of such behaviour requires experimental investigations that detect significant geometric and material nonlinearities. Consequently, the associated constitutive laws are quite complex. Hyper-elastic models are often used to fit nonlinear quasi-static force–deflection curves. Numerous specific formulations of strain energy functions have been proposed to describe the hyper-elastic properties of incompressible as well as compressible materials. A partial overview can be found in Ref. [1]. Phenomenological models include the generalised Rivlin model and the Ogden model. Other models are based on statistical theory in which vulcanised rubber is regarded as a three-dimensional network of long chain molecules connected at a several points.

The theory of linear visco-elasticity is used to model the rate-dependent properties of rubber. Linearity and the Boltzmann superposition principle provide a hereditary integral that represents memory effects observed in creep and relaxation experiments carried out on elastomers [2]. For incompressible materials like rubber, an integral relates isochoric stress to isochoric strain. Incompressibility yields a non-determined hydrostatic pressure. Visco-elastic material models are often constructed by analogy with spring and dash-pot systems [3]. Relaxation kernels are traditionally approximated by the superposition of rheological elements (linear springs and dampers). These models can also be formulated using fractional rheological elements. The main advantage of the fractional derivative model is that it reduces the number of parameters to be identified [4]. Both rheological and fractional models provide very good agreement with the frequency dependence observed in the dynamic modulus. In recent years, many authors have introduced rate-independent friction in one-dimensional models to take into account amplitude dependency. A combined viscous and frictional model is obtained by adding ''friction elastic'' elements to the generalised Maxwell model. This approach is widely used in automotive engineering [5]. Most of these models are of unidirectional macroscopic type and cannot be generalised easily to incorporate multidimensional loading. Moreover they remain linear i.e., they are unable to predict amplitude dependency and nonlinearities due to heavy strains.

The theory of nonlinear visco-elasticity must be used to take into account finite strains and small harmonic oscillations superposed on large static displacements. Pipkin [6] and Lockett [7] gave the general form of the nonlinear visco-elastic function, taking into account isotropy and incompressibility. In Refs. [8–10], nonlinear visco-elastic models are linearised to take into account small harmonic oscillations superposed on large static ones. As discussed by many authors [11,12], all these constitutive equations can be implemented in finite element models and many algorithms have been developed for this purpose, but the high number of degrees of freedom (dof) necessary makes the procedure complex.

The main objective of this article is to propose two models using simplified approximations based either on a rheological formulation, or on the restoring force model for the possible prediction of the harmonic response of a structure equipped with elastomer specimens. In this paper the aim is to obtain the dynamic modulus extracted from the two proposed theoretical approaches and compare them to the experimental results. Section 2 presents an equivalent rheological model using only a few dof. In particular the dynamic modulus is provided by a

Volterra development of the visco-elastic constitutive law. Section 3 is devoted to the description of the restoring force model and establishes the force–deflection loops from which the dynamic modulus can be extracted. Then, the two proposed approaches are applied to traction–compression tests carried out on an elastomer mount with a small quantity of carbon black filler (see Section 4) and to shear tests performed on elastomer plates with a large quantity of black filler (see Section 5).

2. Equivalent rheological model

The behaviour of an elastomer specimen obviously depends on its geometry and constitutive material. The proposed rheological model uses only a few dof and a constitutive law.

2.1. Constitutive equation

Stress is expressed as a function of strain history. Green and Rivlin [13–15] derived integral approximations for this function by using the Weierstrass theorem on the polynomial approximation of continuous functions. Pipkin [6] proposed a generic form of the development, expanded as a 3-order Volterra series containing one-dimensional kernels to take into account isotropy and incompressibility. This form has also been used by Lockett [7] to discuss experiments carried out to identify relaxation kernels. Following Refs. [6,7], the constitutive equation is formulated as follows:

$$S_{ij}(t) = -p(t)C_{ij}^{-1} + S_{ij}^{1}(t) + S_{ij}^{2}(t) + S_{ij}^{3}(t), \tag{1}$$

where $p(t)$ is a non-determined hydrostatic pressure, C_{ij} are the components of the right Cauchy–Green tensor and $S_{ij}^{1}, S_{ij}^{2}, S_{ij}^{3}$ are the components of the 3-order Volterra series of the second Piola–Kirchoff stress tensor linked to the Green–Lagrange strain tensor $\mathbf{E}(t)$ by the following equation:

$$S_{ij}^{1}(t) = \int_{-\infty}^{t} r_1(t-\tau)\dot{E}_{ij}(\tau)\,\mathrm{d}\tau,$$

$$S_{ij}^{2}(t) = \int_{-\infty}^{t}\int_{-\infty}^{t} r_2(t-\tau_1, t-\tau_2)\dot{E}_{ik}(\tau_1)\dot{E}_{kj}(\tau_2)\,\mathrm{d}\tau_1\,\mathrm{d}\tau_2,$$

$$\begin{aligned} S_{ij}^{3}(t) = {} & \int_{-\infty}^{t}\int_{-\infty}^{t}\int_{-\infty}^{t} r_{31}(t-\tau_1, t-\tau_2, t-\tau_3)\mathrm{trace}(\dot{E}_{ik}(\tau_1)\dot{E}_{kl}(\tau_2))\dot{E}_{lj}(\tau_3)\,\mathrm{d}\tau_1\,\mathrm{d}\tau_2\,\mathrm{d}\tau_3 \\ & + \int_{-\infty}^{t}\int_{-\infty}^{t}\int_{-\infty}^{t} r_{32}(t-\tau_1, t-\tau_2, t-\tau_3)\dot{E}_{ik}(\tau_1)\dot{E}_{kl}(\tau_2)\dot{E}_{lj}(\tau_3)\,\mathrm{d}\tau_1\,\mathrm{d}\tau_2\,\mathrm{d}\tau_3, \end{aligned} \tag{2}$$

where $r_k(t_k)$ are the relaxation kernels that link the deviatory stress matrix components with the strain. Constant kernels reduce the development to nonlinear elastic behaviour. Linear visco-elasticity corresponds to the first term of the development, where the first kernel $r_1(t)$ is a monotonic function of t, with $r_1(\infty) \neq 0$ being used to capture the elastic response. This kernel is classically approximated by using a Prony series [16] or fractional derivative models [4]. The

second- and third-order relaxation functions can be approximated by using a decreasing exponential [17].

2.2. Rayleigh–Ritz expansion

According to the Rayleigh–Ritz method, the displacement $\mathbf{u}$ and the virtual displacement $\mathbf{u}^*$ of a point M are expanded as a linear combination of a chosen and admissible kinematic displacement function matrix $\Phi(M)$,

$$u_j(M,t) = \alpha_k(t)\Phi_j^k(M), \quad u_j^*(M,t) = \alpha_k^*(t)\Phi_j^k(M) \quad \forall M(x_1,x_2,x_3), \tag{3}$$

where $\boldsymbol{\alpha}$ and $\boldsymbol{\alpha}^*$ are the vector and the virtual vector, respectively, of the kinematical parameters.

The approximation based on only one kinematic displacement field Φ_j, yields the following approximation of the Green–Lagrange strain tensor:

$$\begin{aligned} E_{ij}(t) &= \frac{1}{2}\left(\frac{\partial u_i(t)}{\partial X_j} + \frac{\partial u_j(t)}{\partial X_i}\right) + \frac{1}{2}\left(\frac{\partial u_k(t)}{\partial X_j}\frac{\partial u_k(t)}{\partial X_i}\right) \\ &= U(t)\tilde{E}_{1ij} + U^2(t)\tilde{E}_{2ij}, \end{aligned} \tag{4}$$

$\tilde{E}_{1ij}$ and $\tilde{E}_{2ij}$ are calculated from the displacement field Φ_j as follows:

$$\tilde{E}_{1ij} = \frac{1}{U_\Phi}\left[\frac{1}{2}\left(\frac{\partial \Phi_i}{\partial X_j} + \frac{\partial \Phi_j}{\partial X_i}\right)\right],$$

$$\tilde{E}_{2ij} = \frac{1}{U_\Phi^2}\left[\frac{1}{2}\left(\frac{\partial \Phi_k}{\partial X_j}\frac{\partial \Phi_k}{\partial X_i}\right)\right], \tag{5}$$

where U_Φ denotes the displacement of the constrained face of the elastomer specimen. In order to obtain an analytical expression of the nonlinear time response, let the principle of virtual work be $W_{\text{int}}^* = W_{\text{ext}}^*$. In the case of a one-dimensional loading, the external virtual work is reduced to

$$W_{\text{ext}}^* = F(t)U_\Phi^*, \tag{6}$$

where U_Φ^* denotes the virtual displacement of the constrained face. Using a material description, the internal mechanical virtual work is written as follows, see also Ref. [1]:

$$W_{\text{int}}^* = \int_{\Omega_0} S_{ij}\frac{\partial u_i^*}{\partial X_j}\,\mathrm{d}\Omega_0 + \int_{\Omega_0}\frac{\partial u_i}{\partial X_k}S_{kj}\frac{\partial u_i^*}{\partial X_j}\,\mathrm{d}\Omega_0, \tag{7}$$

where Ω_0 stands for the volume in the non-deformed configuration. Hence, including approximation (3) in the principle of virtual work yields an expression of the nonlinear force:

$$F(t) = \int_{\Omega_0} S_{ij}\tilde{E}_{1ij}\,\mathrm{d}\Omega_0 + 2U(t)\int_{\Omega_0} S_{ij}\tilde{E}_{2ij}\,\mathrm{d}\Omega_0. \tag{8}$$

Experimental dynamic results from a non-pre-loaded specimen permit fitting the parameters of the model. This corresponds to the case of nonlinear viscoelasticity, where nonlinearities are purely constitutive. Since there are no large strains, the second-order terms in the Green–Lagrange strain tensor are not taken into account. Therefore $\mathbf{S} = \boldsymbol{\sigma}$, and only the terms from the linear part of the mechanical internal work are taken into account in the expression of the internal

virtual work. Under these assumptions, Eq. (8) is reduced to

$$F(t) = a_1 \int_{-\infty}^{t} r_1(t-\tau)\dot{U}(\tau)\,\mathrm{d}\tau + b_2 \int_{-\infty}^{t}\int_{-\infty}^{t} r_2(t-\tau_1, t-\tau_2)\dot{U}(\tau_1)\dot{U}(\tau_2)\,\mathrm{d}\tau_1\,\mathrm{d}\tau_2 + c_{31} \int_{-\infty}^{t}\int_{-\infty}^{t}\int_{-\infty}^{t} r_{31}(t-\tau_1, t-\tau_2, t-\tau_3)\dot{U}(\tau_1)\dot{U}(\tau_2)\dot{U}(\tau_3)\,\mathrm{d}\tau_1\,\mathrm{d}\tau_2\,\mathrm{d}\tau_3 + c_{32} \int_{-\infty}^{t}\int_{-\infty}^{t}\int_{-\infty}^{t} r_{32}(t-\tau_1, t-\tau_2, t-\tau_3)\dot{U}(\tau_1)\dot{U}(\tau_2)\dot{U}(\tau_3)\,\mathrm{d}\tau_1\,\mathrm{d}\tau_2\,\mathrm{d}\tau_3, \tag{9}$$

where a_1, b_2, c_{31} and c_{32} are known parameters which take into account the geometry

$$a_1 = \int_{\Omega_0} \tilde{E}_{1ij}\tilde{E}_{1ij}\,\mathrm{d}\Omega_0, \quad b_2 = \int_{\Omega_0} \tilde{E}_{1ik}\tilde{E}_{1kj}\tilde{E}_{1ij}\,\mathrm{d}\Omega_0,$$

$$c_{31} = \int_{\Omega_0} \mathrm{trace}\,(\tilde{E}_{1_{ik}}\tilde{E}_{1_{kl}})\tilde{E}_{1_{lj}}\tilde{E}_{1_{ij}}\,\mathrm{d}\Omega_0, \quad c_{32} = \int_{\Omega_0} \tilde{E}_{1_{ik}}\tilde{E}_{1_{kp}}\tilde{E}_{1_{pj}}\tilde{E}_{1_{ij}}\,\mathrm{d}\Omega_0. \tag{10}$$

2.3. Dynamic modulus

The dynamic modulus is calculated using a harmonic displacement assumption:

$$U(t) = \tfrac{1}{2}(U_0 \mathrm{e}^{\mathrm{i}\omega t} + \bar{U}_0 \mathrm{e}^{-\mathrm{i}\omega t}). \tag{11}$$

The force is calculated from Eq. (9), by using the harmonic balance method. Restricting the development to the first harmonic, the only terms that remain are those from the first and the third kernels. There is no term associated with the fundamental harmonic coming from the second-order kernel, and the dynamic modulus can be written as follows:

$$K(\omega, U_0) = \frac{F(\omega, U_0)}{U_0} = a_1 \mathrm{i}\omega K_1(\omega) + \frac{1}{4}\,\mathrm{i}\omega^3 |U_0|^2 (c_{31}K_{31}(\omega) + c_{32}K_{32}(\omega)), \tag{12}$$

where $K_k(\omega)$ are related to the Fourier transform of the relaxation kernels using the following relationships:

$$K_1(\omega) = \int_0^{\infty} r_1(X)\mathrm{e}^{-\mathrm{i}\omega X}\,\mathrm{d}X,$$

$$K_{3k}(\omega) = \tilde{K}_{3k}(\omega, \omega, -\omega) + \tilde{K}_{3k}(\omega, -\omega, \omega) + \tilde{K}_{3k}(-\omega, \omega, \omega),$$

$$\tilde{K}_{3k}(\omega_1, \omega_2, \omega_3) = \int_0^{\infty}\int_0^{\infty}\int_0^{\infty} r_{3k}(X_1, X_2, X_3)\mathrm{e}^{-\mathrm{i}\omega X_1}\mathrm{e}^{-\mathrm{i}\omega X_2}\mathrm{e}^{-\mathrm{i}\omega X_3}\,\mathrm{d}X_1\,\mathrm{d}X_2\,\mathrm{d}X_3. \tag{13}$$

Hence, for any geometry, the dynamic modulus can be written as a function of the frequency and the amplitude. Eq. (12) can be written as follows:

$$K(\omega, U_0) = K_{\mathrm{Lin}}(\omega) + |U_0|^2 K_{\mathrm{NL}}(\omega), \tag{14}$$

where $K_{\mathrm{Lin}}(\omega)$ and $K_{\mathrm{NL}}(\omega)$, deduced from Eqs. (12) and (13), need to be estimated experimentally for each forcing frequency. In order to evaluate these functions, q experimental tests were carried

out at different levels of displacement which gave $K(\omega, U_i)$ with $i = 1, 2, \ldots, q$. Then, $K_{\mathrm{Lin}}(\omega)$ and $K_{\mathrm{NL}}(\omega)$ were obtained by means of the equation:

$$\begin{bmatrix} 1 & U_1^2 \\ \vdots & \vdots \\ 1 & U_q^2 \end{bmatrix} \begin{Bmatrix} K_{\mathrm{Lin}}(\omega) \\ K_{\mathrm{NL}}(\omega) \end{Bmatrix} = \begin{Bmatrix} K(\omega, U_1) \\ \vdots \\ K(\omega, U_q) \end{Bmatrix} \tag{15}$$

which is solved by a Moore–Penrose inversion. The number of tests q has to be greater than two so that the solution can be compared to a least square approximation.

3. Restoring force model

Elastomer specimens have a hysteretic behaviour that can be described by a global force–deflection loop [18–22]. Existing models are limited when they are formulated from the envelope curves of the loop, which can be time and velocity dependent. Coulomb's model is too simple. Dalh's model has constant envelope lines while the models of Krasnosel'skii and Duhem-Madelung are much too general, see Ref. [23]. Bouc's [24] and Wen's model [25,26] are difficult to formulate from the envelope curves.

3.1. General restoring force model

In Ref. [27], an original and general hysteretic operator for modelling the force–deflection loop is presented. It can model various shapes of possible behaviour: softening, hardening or a combination of both. A simplified formulation permits expressing it as follows:

$$\frac{\mathrm{d}R}{\mathrm{d}t} = \beta \frac{\mathrm{d}u}{\mathrm{d}t} \left(h - R \operatorname{sgn}\left(\frac{\mathrm{d}u}{\mathrm{d}t} \right) \right) \tag{16}$$

with u being the deflection, β a constant, h the following equation:

$$h = \frac{1}{2} \left((h_u + h_l) \operatorname{sgn}\left(\frac{\mathrm{d}u}{\mathrm{d}t} \right) + (h_u - h_l) \right) \tag{17}$$

containing the upper h_u and lower h_l envelope curves between which the restoring force R must remain. Measurement of the force–deflection loops permits the identification of these parameters, in particular the envelope curves.

The response of a structure equipped with such a specimen is easily predicted by coupling the first differential equation of the restoring force model (16) with the second-order differential equations governing the behaviour of the structure and containing the restoring force in their second member. A step-by-step time integration scheme permits predicting the transient and harmonic forced response [28].

3.2. Dynamic modulus

In order to collect and compare common results with the equivalent rheological model, the dynamic equivalent stiffness modulus can be extracted from the force–deflection loops established with the proposed restoring force model. Classically, harmonic investigation requires the use of dynamic equivalent stiffness k_e and loss factor η_e, which are assumed to be constant during one cycle. They are extracted from the simulated and measured loops using the following classical formulae:

$$k_e = \frac{R_{\max} - R_{\min}}{u_{\max} - u_{\min}}, \tag{18}$$

$$\eta_e = \frac{(R_{\max} - R_{\min})|_{u=0}}{R_{\max} - R_{\min}} \tag{19}$$

which permit expressing complex stiffness k:

$$k = k_e(1 + \mathrm{j}\eta_e) \tag{20}$$

or

$$k = k_r + \mathrm{j}k_i \tag{21}$$

with $\mathrm{j} = \sqrt{-1}$.

4. Elastomer specimen under traction–compression tests

4.1. Experimental investigation

The traction–compression tests, see Figs. 1 and 2, were carried out on a cylindrical mount made of carbon black filled rubber (diameter, 43 mm; height, 60 mm). Fixed at one of its ends, it was subjected to axial harmonic deflection with different amplitudes and forcing frequencies. The quasi-static tests were performed with a frequency of 0.0032 Hz and a 19 mm triangular deflection amplitude while the dynamic tests were performed with a 10–50 Hz swept sine deflection for several amplitudes from 0.2 to 1.0 mm. The complex modulus $K(\omega, \beta_0)$ is evaluated by computing the ratio between the harmonic input displacement $U(t) = \beta_0 \mathrm{e}^{\mathrm{i}\omega t}$ and the associated output force $F(t) = F_0 \mathrm{e}^{\mathrm{i}\omega t}$ on the same harmonic. The swept sine tests permit obtaining the global nonlinear behaviour across the entire frequency band.

From the measurement of the dynamic modulus, it can be concluded that both frequency and amplitude dependencies exist. The dynamic modulus increases with frequency, see Fig. 3, which is clearly due to viscous dissipation, and decreases with amplitude, see Fig. 4. The rubber used for the compression specimen contains very little carbon black filler. The damping properties of this type of material are amplitude quasi-independent.

4.2. Dynamic modulus from the equivalent rheological model

The Volterra development predicts the general form of the dynamic modulus expressed by formula (14), as a function of the amplitude and the frequency, in the case of harmonic response

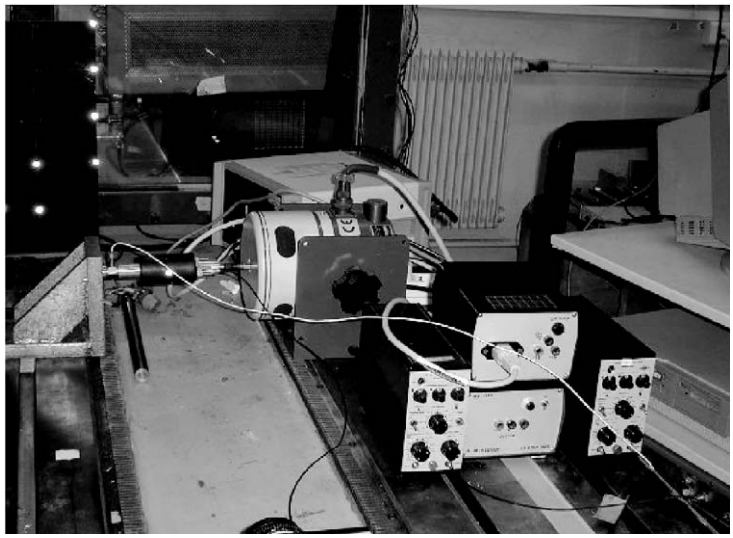

Fig. 1. Photo of the traction–compression test rig.

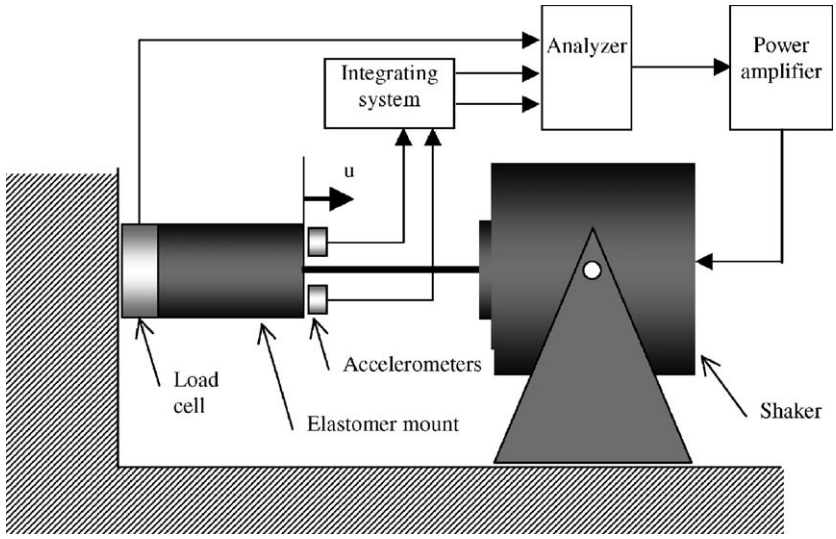

Fig. 2. Block diagram of the traction–compression test rig.

and of a nonlinear viscoelastic specimen. It has been demonstrated [29] that the harmonic test is very sensitive to nonlinearities and permits identifying the Volterra series.

Let n, p and k represent three different amplitude levels of the forcing deflection. The following function

$$g_k(\omega, n) = \frac{K_n(\omega) - K_p(\omega)}{K_k(\omega) - K_p(\omega)} \tag{22}$$

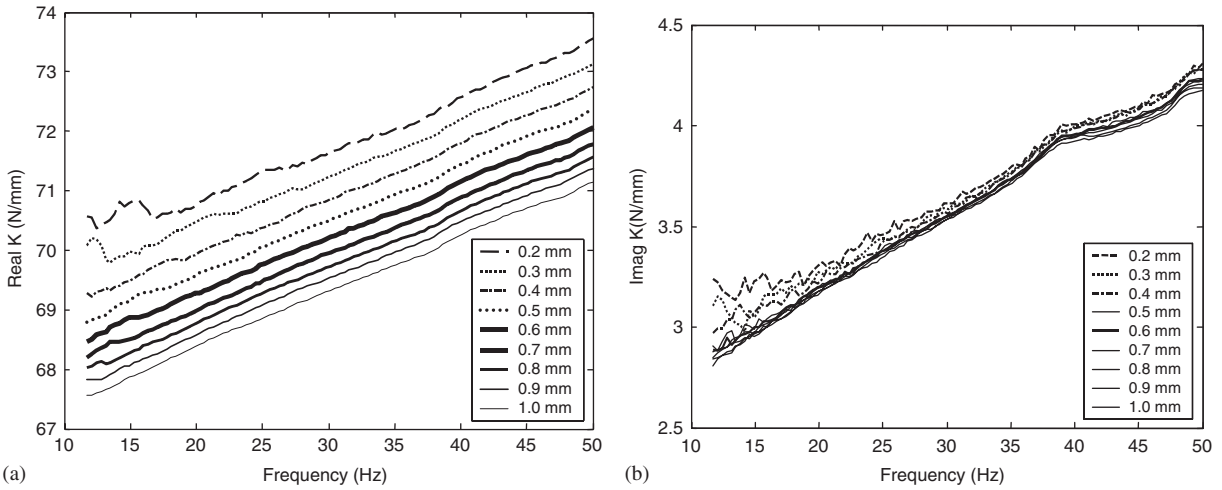

Fig. 3. Traction–compression tests. Measured real (a) and imaginary (b) parts of the dynamic modulus versus forcing frequency.

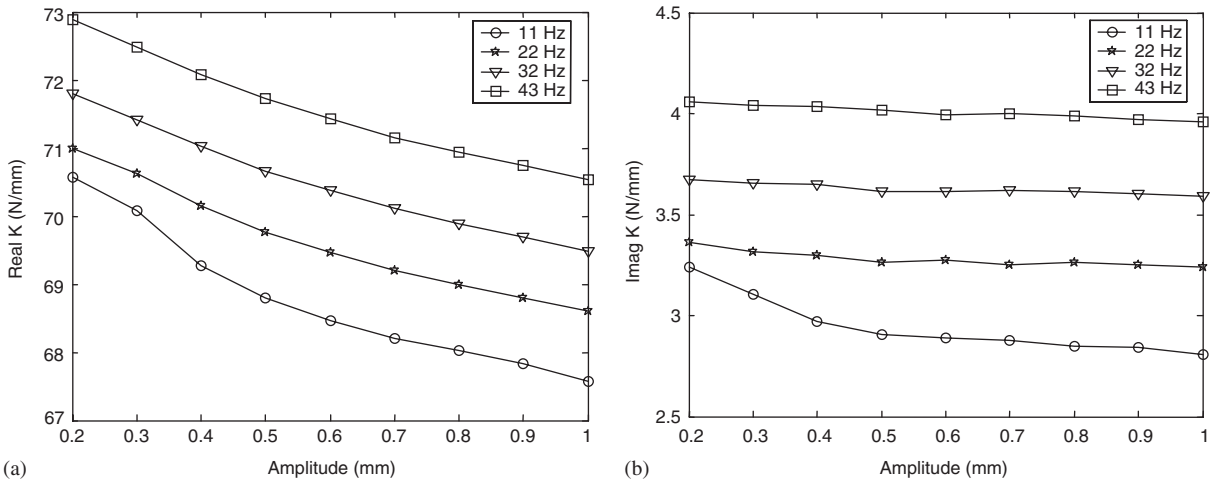

Fig. 4. Traction–compression tests. Measured real (a) and imaginary (b) parts of the dynamic modulus versus deflection amplitude.

is plotted in Fig. 5 for several values of n. Parameters k and p are fixed to 1 and 0.2 mm, respectively. The results highlight that the evolutions of the real part of g_1 are relatively constant versus frequency and confirm that the amplitude and frequency dependencies are uncoupled. For each forcing frequency, the values of $K_{\mathrm{Lin}}(\omega)$ and $K_{\mathrm{NL}}(\omega)$ that minimize the error with experimental data are sought, see Eq. (15) and Fig. 6.

Thus it can be claimed that the Volterra expansion permits obtaining the dynamic modulus as a function of the amplitude with good accuracy, at least for a specimen with very few little carbon black filler.

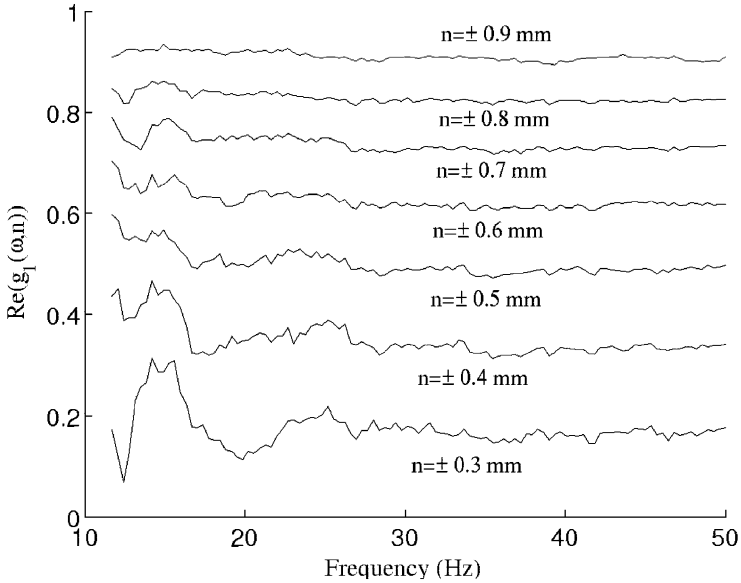

Fig. 5. Traction–compression test, with no pre-load. Real part of Eq. (22) with $p = 0.2$ and $k = 1$.

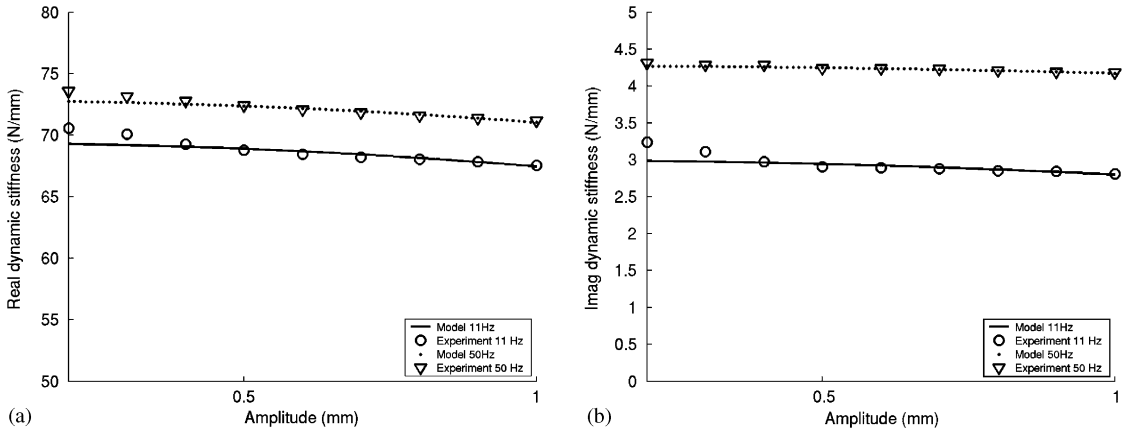

Fig. 6. Traction–compression test. Real (a) and imaginary (b) parts of the dynamic modulus measured and predicted with the rheological approach.

4.3. Dynamic modulus from the restoring force model

The experimental quasi-static loop permits identifying the parameters of the restoring force model. The triangular deflection is approximated with a Fourier series using 10 coefficients to obtain the velocity and its sign, see Fig. 7, and to take into account the successive cycles

$$\frac{u}{u_c} = \frac{2}{\pi^2} \sum_{n=0}^{10} \frac{1}{(2n+1)^2} \cos\left(2\pi f(2n+1)\left(t + \frac{1}{4f}\right)\right), \tag{23}$$

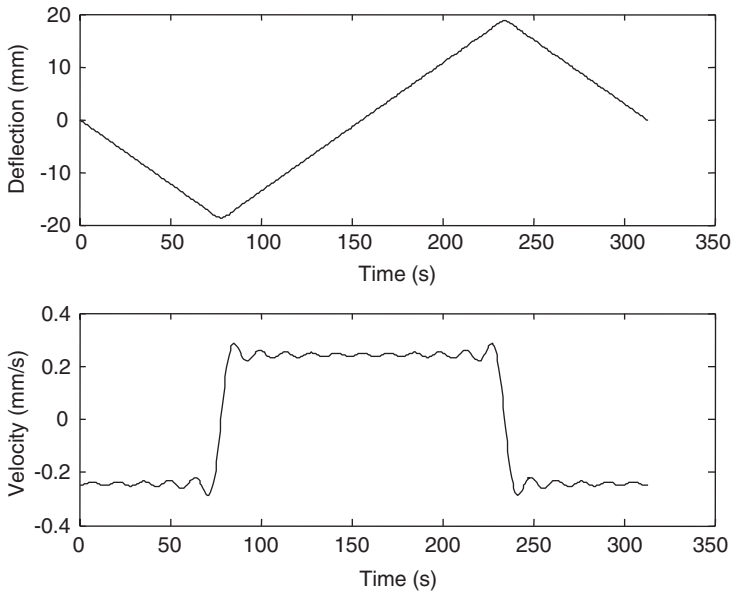

Fig. 7. Approximated time history triangular deflection and its time derivative for the traction–compression test.

where u_c is the maximum deflection of each loop while f is the forcing frequency. Constant β is adjusted at 6000 by comparing the areas of the measured and predicted loops while the envelope curves are approximated by using the least-square method:

$$h_u = \left(-794560u^2 + 47280u + 71.783 - 50\left(1 - \frac{u_c}{0.019}\right)^2\right)(0.741 + 0.005f), \tag{24}$$

$$h_l = \left(-583400u^2 + 49012u - 47.769 + 18\left(1 - \frac{u_c}{0.019}\right)^2\right)(0.741 + 0.005f). \tag{25}$$

The quasi-static force–deflection loops of the elastomer cylinder mount measured and predicted by using relations (16), (17), (23), (24) and (25) are compared in Fig. 8.

The harmonic force–deflection loops dependant on forcing frequency f are plotted in Figs. 9a and b for an 11 and 50 Hz forcing frequency. The global slope of the loop increases with the forcing frequency. This is also described by Figs. 9c and d, which show the extracted real and imaginary parts of the complex stiffness by using relations (18)–(21). The restoring force model proposed satisfactorily describes the experimental harmonic behaviour of the cylindrical mount under traction–compression.

The hardening–softening behaviour of the loops plotted in Figs. 8 and 9a is mainly due to the geometric configuration imposed by the compression–traction test.

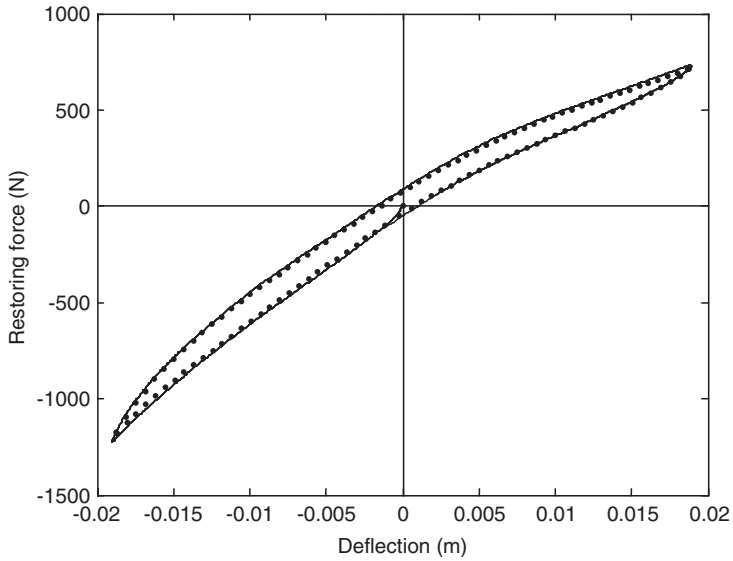

Fig. 8. Traction–compression test at $f = 0.0032$ Hz. Quasi-static force–deflection loops measured (solid line) and predicted (dotted line) with the restoring force model.

5. Elastomer specimen under shear tests

5.1. Experimental investigation

The shear tests were carried out on a pair of elastomer (also carbon black filled rubber) plates placed opposite each other, see Fig. 10.

They were subjected to axial harmonic deflection having different amplitudes and forcing frequencies. Only a positive triangular deflection was applied for the quasi-static test (frequency of 0.01 Hz and amplitude of 3.5 mm). The dynamic tests were performed using a sine excitation with a (10–100 Hz) frequency range and an (0–1.0 mm) amplitude range.

The shear specimen contained more carbon black filler than the specimen used for the compression test. The measurement of the dynamic modulus shows that amplitude dependency is more pronounced for this specimen and that the evolution of the dynamic modulus function of the amplitude is substantially nonlinear, see Fig. 11.

5.2. Dynamic modulus from equivalent rheological model

Formula (22) is investigated again in the case of the shear test. The quasi-constant changes of the real and imaginary parts of function g_k show that the amplitudes and frequency dependencies can be uncoupled even if the specimen is heavily filled rubber, see Fig. 12.

For each forcing frequency, the values of $K_{\mathrm{Lin}}(\omega)$ and $K_{\mathrm{NL}}(\omega)$ which minimize the error with the experimental data are sought, see Eq. (15). A Volterra expansion to order 3 predicts a

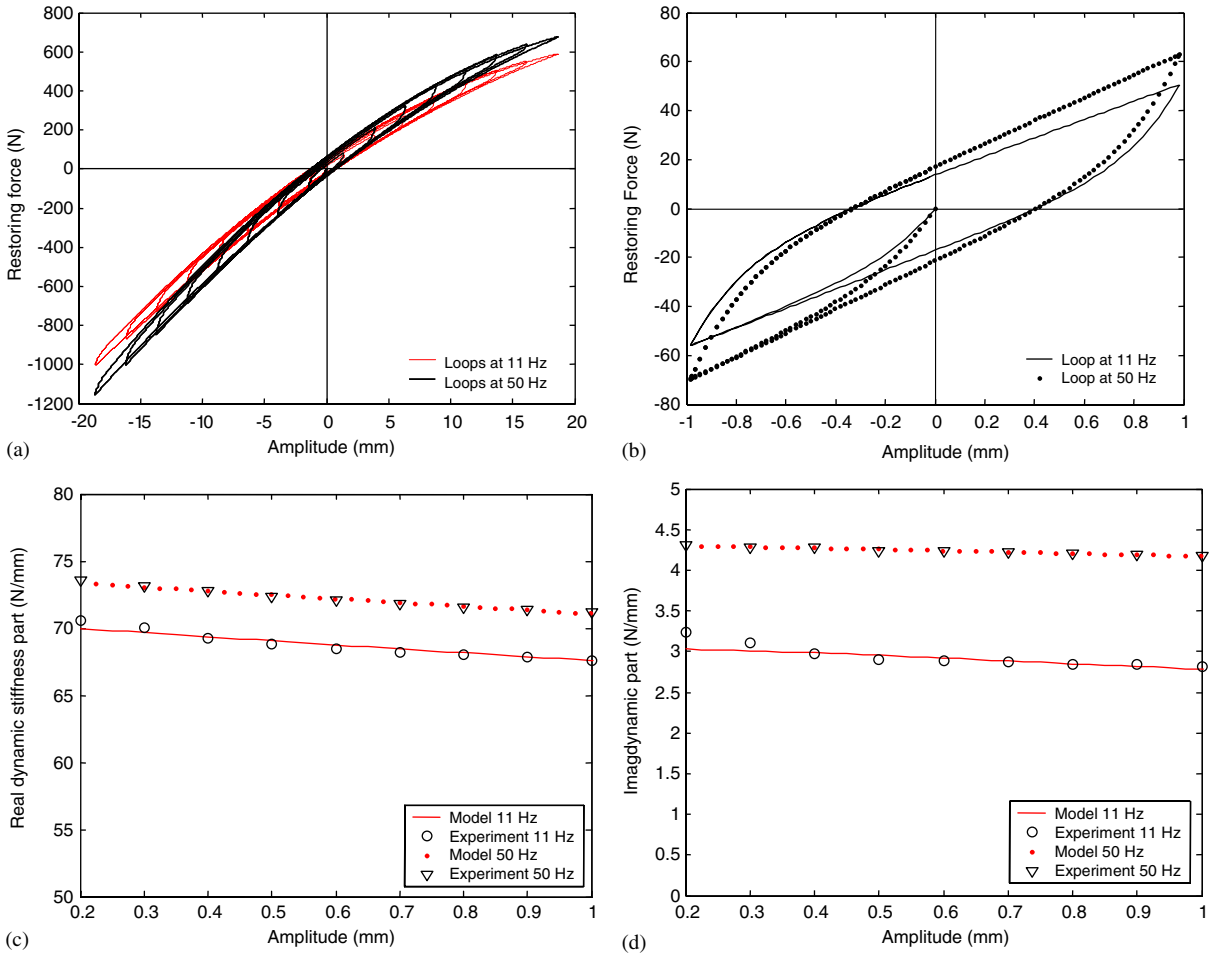

Fig. 9. Traction–compression test at 11 and 50 Hz. Force–deflection loops versus 1.5–19 mm (a) and 1 mm (b) deflection amplitudes. Real (c) and imaginary (d) parts of the dynamic modulus measured and predicted with the restoring force model.

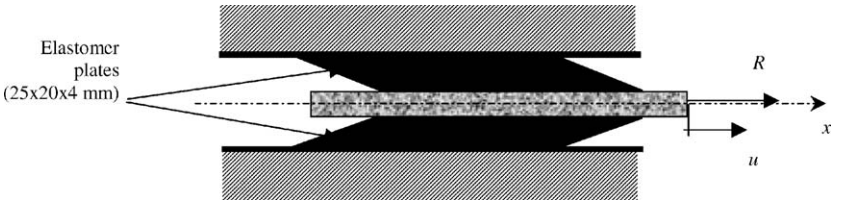

Fig. 10. Elastomer plates subjected to a shear test.

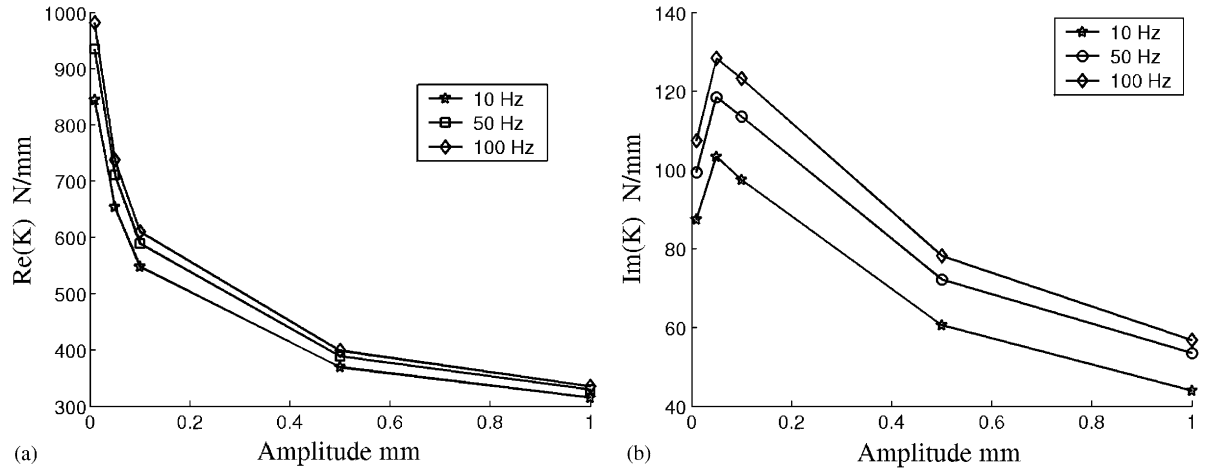

Fig. 11. Shear test. Measured real (a) and imaginary (b) parts of the dynamic modulus versus deflection for several frequencies.

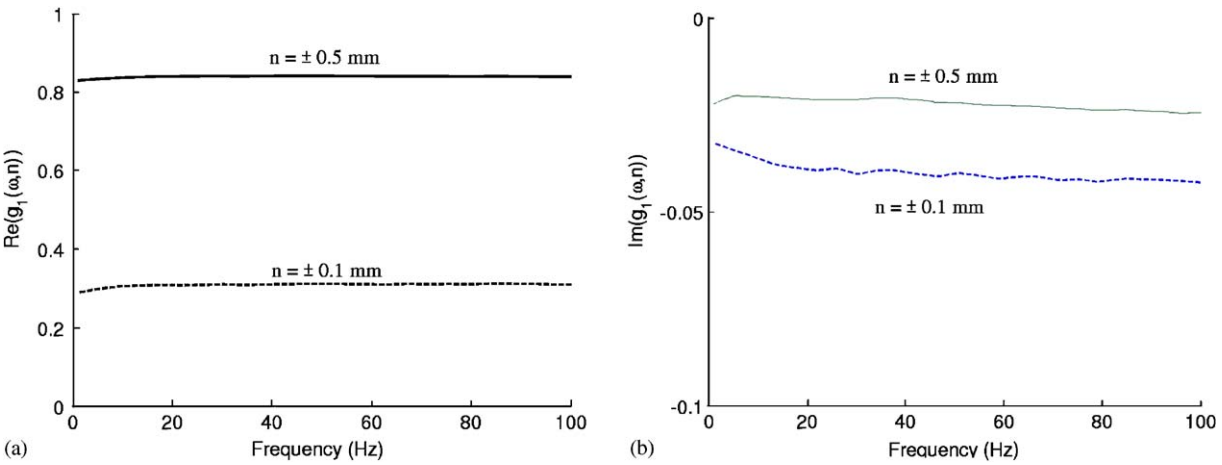

Fig. 12. Shear test, with no pre-load. Real (a) and imaginary (b) parts of Eq. (22) with $p = 0.05$ and $k = 1$.

quadratic dependency on amplitude. This expansion is not satisfactory, see Fig. 13, since the convexities of the predicted and measured dynamic modulus versus amplitude oppose each other. One solution to this is to use more than three kernels, which is computer time consuming while another possibility is to develop the function using creep kernels instead of relaxation kernels.

Let the inversion of expression (9) yield the following expression for the velocity:

$$\dot{U}(t) = \int_0^\infty h_1(\tau)F(t-\tau)\,\mathrm{d}\tau + \int_0^\infty \int_0^\infty h_2(\tau_1,\tau_2)F(t-\tau_1)F(t-\tau_2)\,\mathrm{d}\tau_1\,\mathrm{d}\tau_2 + \int_0^\infty \int_0^\infty \int_0^\infty h_3(\tau_1,\tau_2,\tau_3)F(t-\tau_1)F(t-\tau_2)F(t-\tau_3)\,\mathrm{d}\tau_1\,\mathrm{d}\tau_2\,\mathrm{d}\tau_3, \quad (26)$$

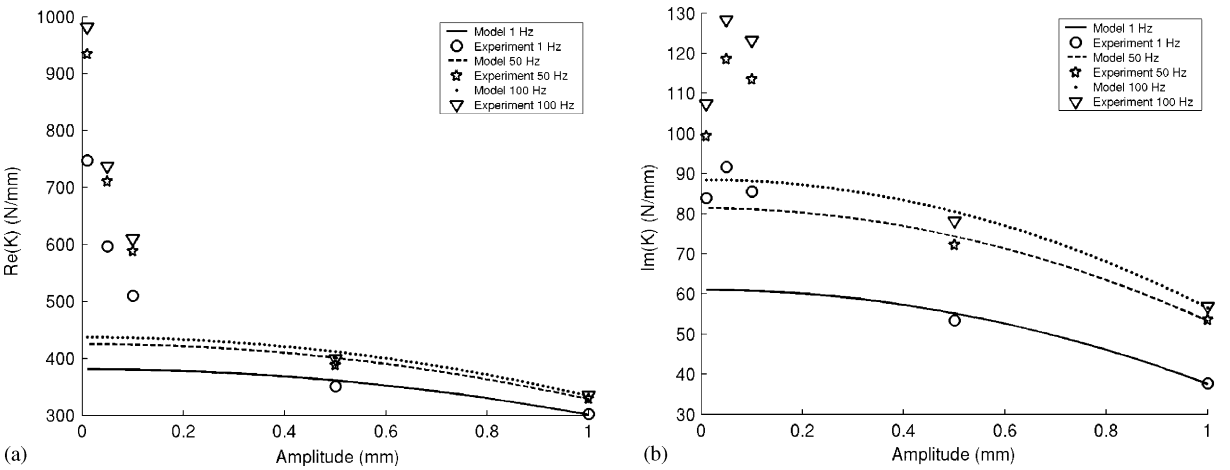

Fig. 13. Shear test and relaxation kernels. Measured and predicted real (a) and imaginary (b) parts of the dynamic stiffness versus deflection for several forcing frequencies.

where h_k are the creep functions. In this case, the form of the dynamic compliance is

$$\frac{U}{F(\omega)} = H(\omega) = H_{\mathrm{Lin}}(\omega) + |F(\omega)|^2 H_{\mathrm{NL}}(\omega), \tag{27}$$

where the corresponding compliances and $H_{\mathrm{Lin}}(\omega)$ and $H_{\mathrm{NL}}(\omega)$ can be calculated from the expression of the Fourier transform of the relaxation functions $K_k(\omega)$ following a procedure detailed in Ref. [12]. A least square method permits finding the values of $H_{\mathrm{Lin}}(\omega)$ and $H_{\mathrm{NL}}(\omega)$ that best fit the compliance deflection curve (for each value of the frequency). Eq. (27) is better adapted than Eq. (14) for describing the deflection amplitude dependency.

The dynamic characteristics extracted from this model are then compared in Figs. 14 and 15 with the measured data. The expansion using creep kernels is satisfactory for the real and the imaginary parts of the stiffness.

5.3. Dynamic modulus from the restoring force model

As in Section 4.3, the experimental quasi-static loop permits adjusting the parameters of the restoring force model: $\beta = 2 \times 10^5$ and the triangular deflection is approximated with a Fourier series using 10 coefficients, see also Fig. 16:

$$\frac{u}{u_c} = \frac{1}{2} - \frac{4}{\pi^2} \sum_{n=0}^{10} \frac{1}{(2n+1)^2} \cos(2\pi f(2n+1)t). \tag{28}$$

Introducing the maximum amplitude makes the curve available for harmonic excitation. To do this, the ordinate axis is divided by the maximum value $h_c \approx 730\,\mathrm{N}$ and the abscissa axis by the

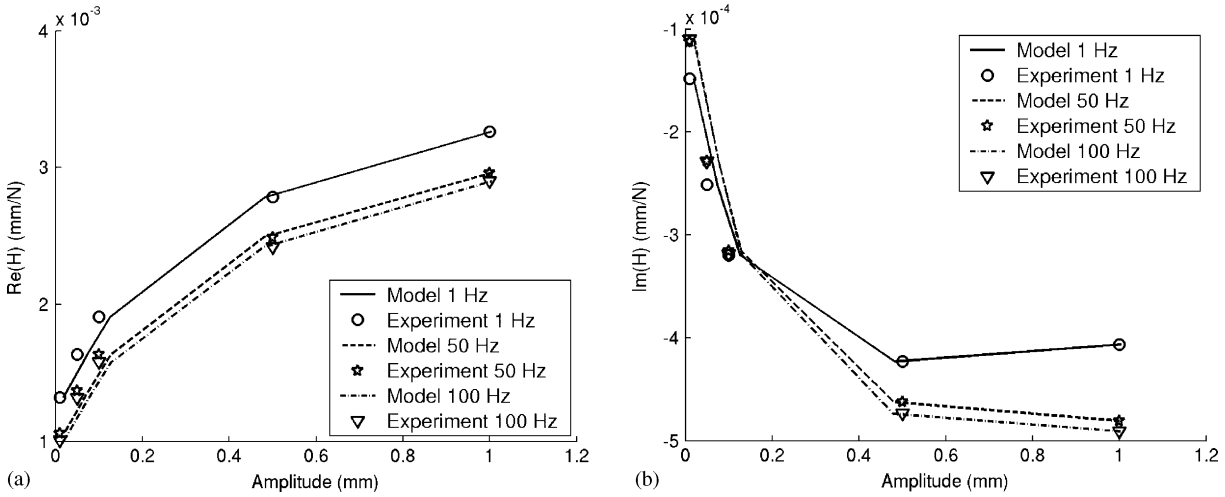

Fig. 14. Shear test and creep kernels. Measured and predicted real (a) and imaginary (b) parts of the dynamic compliance versus deflexion for several frequencies.

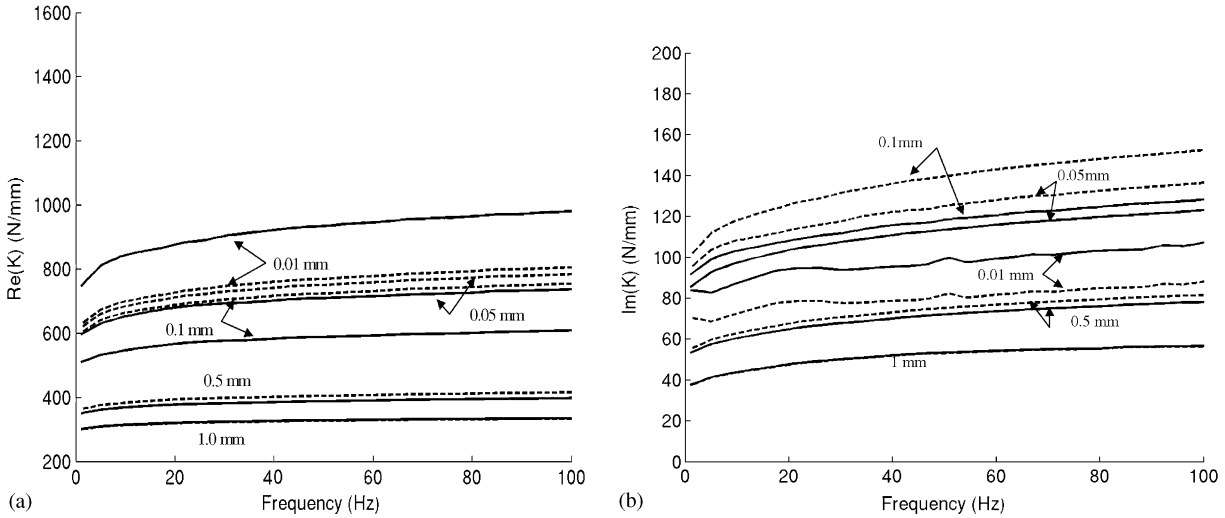

Fig. 15. Shear test and creep kernels. Measured (dashed line) and predicted (solid line) real (a) and imaginary (b) parts of the dynamic stiffness.

maximum deflection $u_c = 0.0035\,\mathrm{m}$. Using the least square method yields:

$$\frac{h_u}{h_c} = 0.71 + 0.36\left(\frac{u}{u_c}\right)^3 - 0.69\mathrm{e}^{-2.20(u/u_c)}, \tag{29}$$

$$\frac{h_l}{h_c} = 0.006 + 0.79\left(\frac{u}{u_c}\right) - 0.00003\mathrm{e}^{8.75(u/u_c)}. \tag{30}$$

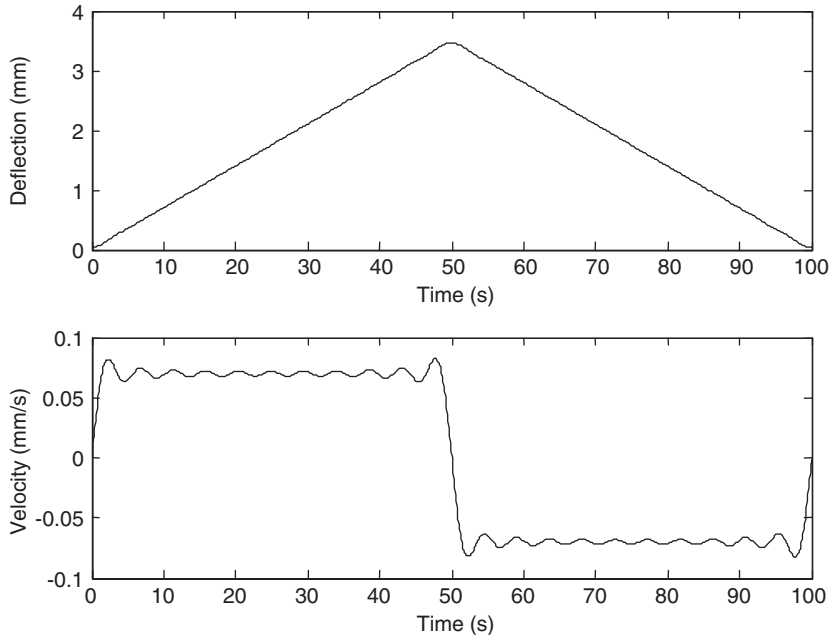

Fig. 16. Fourier series of the time history triangular deflection and its time derivative for the shear test.

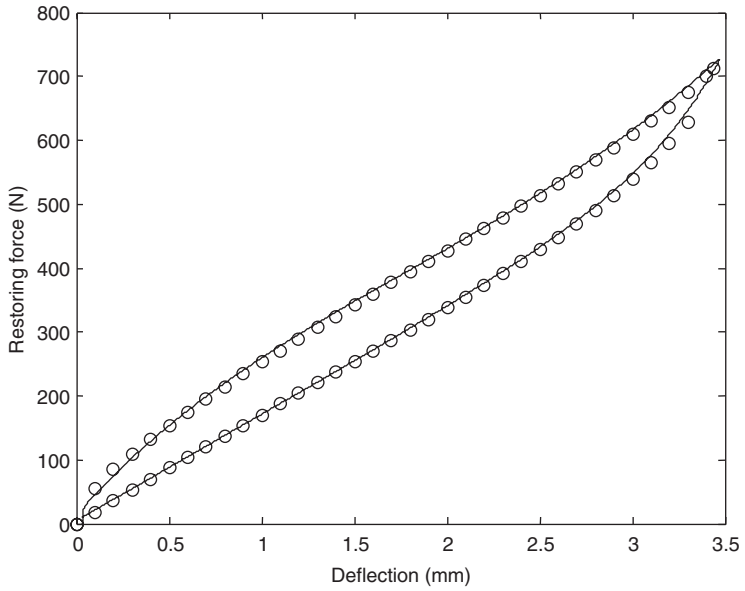

Fig. 17. Shear test. Maximum force–deflection loops measured (dotted line) and predicted (solid line) with the restoring force model.

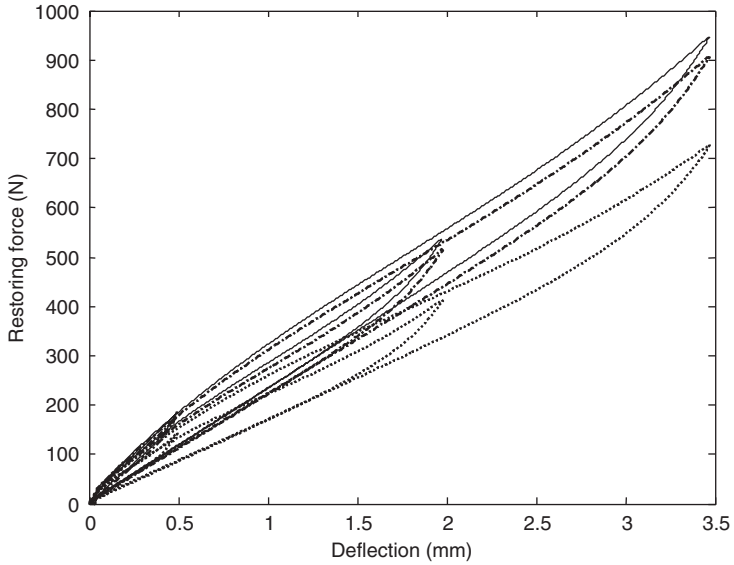

Fig. 18. Shear test. Predicted force–deflection loops with the restoring force model for two maximum amplitudes (dotted lines: 0.01 Hz, dashed lines: 50 Hz, solid lines: 100 Hz).

Fig. 17 permits comparing the maximum force–deflection loop measured and predicted by using relations (16), (17), (29) and (30).

In order to take into account the frequency effect in the absence of experimental loops, it can be assumed that the loop rotates with a quadratic evolution of the frequency. See the measured dynamic equivalent stiffness plotted in Fig. 11, which increases with the forcing frequency. Consequently, relations (29) and (30) become

$$\frac{h_u}{h_c} = 0.71 + 0.36\left(\frac{u}{u_c}\right)^3 - 0.69\mathrm{e}^{-2.20(u/u_c)} + \frac{u}{u_c}(0.007f - 0.00004f^2), \tag{31}$$

$$\frac{h_l}{h_c} = 0.006 + 0.79\left(\frac{u}{u_c}\right) - 0.00003\mathrm{e}^{8.75(u/u_c)} + \frac{u}{u_c}(0.007f - 0.00004f^2). \tag{32}$$

Fig. 18 shows the loops for several deflection amplitudes and forcing frequencies.

Considering several positive harmonic deflection amplitudes (0.01, 0.05, 0.1, 0.5, and 1 mm) and three forcing frequencies (10, 50 and 100 Hz), the equivalent dynamic stiffnesses extracted from the model, see Eqs. (16)–(21), (31) and (32), are compared with the measured real stiffness in Figs. 19 and 20. The restoring force model is satisfactory except for the very lowest deflection amplitude (0.01 mm), see Fig. 20, from which it is difficult to establish the model, since the measured loops are too small.

Regarding the shear test performed for the positive deflection amplitude only, formula (19) cannot be used for evaluating the equivalent loss factor.

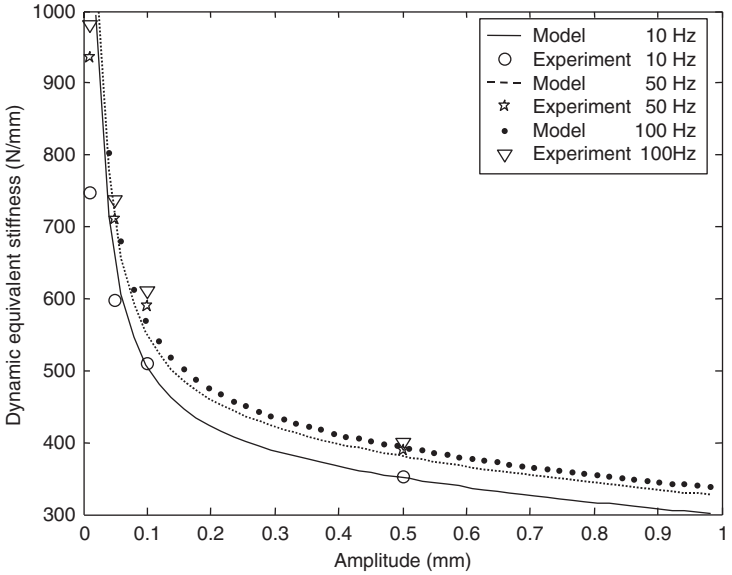

Fig. 19. Shear test. Dynamic equivalent stiffness measured and predicted with the restoring force model.

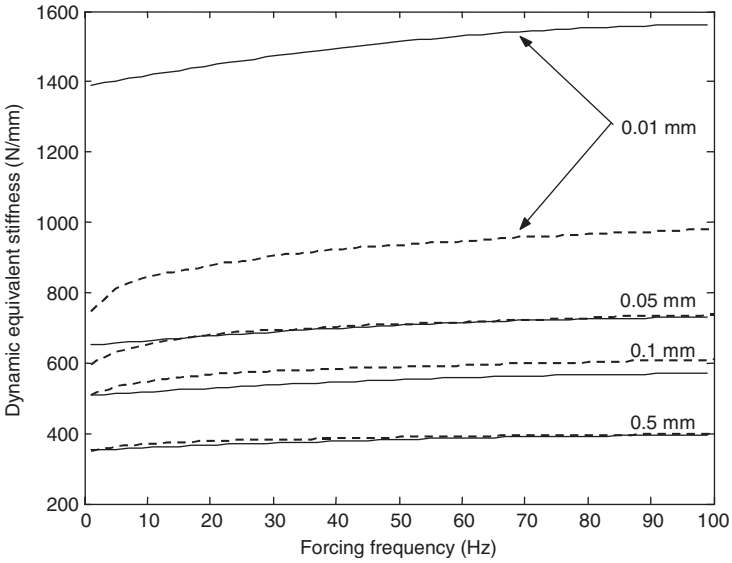

Fig. 20. Shear test. Dynamic equivalent stiffness measured (dashed line) and predicted with the restoring force model (solid line).

6. Conclusion

The visco-elastic behaviour of elastomer specimens was described using either an equivalent rheological model or a restoring force model. The comparison of the dynamic modulus extracted

from the two models and from the experimental investigation permits validating the two theoretical approaches.

In the rheological approach, the constitutive laws are expanded by a Volterra series using three one-dimension kernels. It was shown that relaxation kernels give a satisfactory predicted dynamic modulus in the case of the traction–compression test which highlights a hardening–softening behaviour of the cylinder. However, relaxation kernels are limited in the case of the shear test, which highlights a hardening–hardening behaviour of the squared plate. In the latter case it is necessary to use a creep kernel to obtain a satisfactory predicted dynamic modulus.

The restoring force model requires experimental force–deflection loops measured for different deflection amplitudes and forcing frequencies. This model can be generalised since its envelope curves can be a function of the deflection amplitude, the forcing frequencies and, if necessary, the pre-load.

Possible prediction of the harmonic response of a structure equipped with elastomer specimens requires:

1. in the case of the equivalent rheological model, introducing the dynamic modulus in the first member of the equations of motion and performing a resolution in the frequency domain,
2. in the case of the restoring force model, incorporating the restoring force obtained with the first-order differential equation in the second member of the equations of the motion and performing a resolution in the time domain, with the restoring force being updated at each time step.

Acknowledgements

The authors would like to thank C.F. Gomma and the Rhône-Alpes Regional Council for their support.

References

[1] G.A. Holzapfel, *Non Linear Solid Mechanics*, Wiley, New York, 2000.
[2] J. Salencon, *Viscoélasticité cours de calcul des structures anélastiques*, Presses de l'Ecole Nationale des Ponts et Chaussées, France, 1983.
[3] J. Lemaitre, J.L. Chaboche, *Mécanique des Matériaux Solides*, Dunod, Paris, 1984.
[4] R.L. Bagley, P. Torvik, On the fractional calculus model of viscoelastic behavior, *Journal of Rheology* 30 (1986) 133–155.
[5] P.E. Austrell, Modeling of Elasticity and Damping for Filled Elastomers, PhD Thesis, Lund University, 1997.
[6] A.C. Pipkin, Small finite deformations of viscoelastic solids, *Reviews of Modern Physics* 36 (1964) 1034–1041.
[7] F. Lockett, Creep and relaxation experiments for non linear materials, *International Journal of Engineering Science* 3 (1965) 59–75.
[8] G. Lianis, Small deformation in viscoelastic bodies, in: *Proceeding of the Fourth International Congress on Rheology*, 1965, pp. 109–119.
[9] K.N. Morman, J.C. Nagtegaal, Finite element analysis of sinusoidal small-amplitude vibrations in deformed viscoelastic solids, *International Journal for Numerical Methods in Engineering* 19 (1983) 1079–1103.
[10] A.B. Zdunek, Theory and computation of the steady state harmonic response of viscoelastic rubber parts, *Computer Methods in Applied Mechanics and Engineering* 105 (1993) 63–92.

[11] S. Reese, S. Govindjee, A theory of finite viscoelasticity and numerical aspects, *International Journal of Solids and Structures* 35 (1998) 3455–3482.
[12] M. Morhac, Determination of inverse Volterra kernels in nonlinear discrete systems, *Nonlinear Analysis Theory* 15 (1990) 269–281.
[13] A.E. Green, R.S. Rivlin, The mechanics of non linear materials with memory, *Archive for Rational Mechanics and Analysis* 1 (1957) 1–21.
[14] A.E. Green, R.S. Rivlin, The mechanics of non linear materials with memory, *Archive for Rational Mechanics and Analysis* 3 (1959) 82–90.
[15] A.E. Green, R.S. Rivlin, The mechanics of non linear materials with memory, *Archive for Rational Mechanics and Analysis* 4 (1959) 387–407.
[16] J.D. Ferry, *Viscoelastic Properties of Polymers*, Wiley, New York, 1980.
[17] A. Soulimani, Une méthode énergétique de modélisation de la viscoélasticité non linéaire en grandes transformations, Thèse de doctorat en mécanique, Ecole Nationale des Ponts et Chaussées, France, 1993.
[18] D. Nashif, D.I.G. Jones, J.P. Henderson, *Vibration Damping*, Wiley, New York, 1985.
[19] D.G. Jones, *Handbook of Viscoelastic Vibration Damping*, Wiley, New York, 2001.
[20] J.B. Roberts, P.D. Spanos, *Random Vibration and Statistical Linearisation*, Wiley, New York, 1990.
[21] K. Gjika, R. Dufour, Rigid body and nonlinear mount identification: application to onboard equipment with hysteretic suspension, *Journal of Vibration and Control* 5 (1) (1999) 75–94.
[22] K. Gjika, R. Dufour, G. Ferraris, Transient response of structures on viscoelastic or elastoplastic mounts: prediction and experiment, *Journal of Sound and Vibration* 198 (3) (1996) 361–378.
[23] P.A. Bliman, Etude mathématique d'un modèle de frottement sec: le modèle de P. R. Dahl, Thèse de doctorat en mathématiques et automatique, University of Paris IX-Dauphine, 1990.
[24] R. Bouc, Forced vibrations of a mechanical system with hysteretic, *Proceedings of the Fourth Conference on Nonlinear Oscillation*, 1967, p. 315.
[25] Y.K. Wen, Method for random vibration of hysteretic system, *Journal of the Engineering Mechanics Division, ASCE* 102 (2) (1976) 249–263.
[26] Y.K. Wen, Equivalent linearisation for hysteretic system under random excitation, *Journal of Applied Mechanics* 47 (1990) 150–154.
[27] A. Al Majid, R. Dufour, Formulation of a hysteretic restoring force model. Application to vibration isolation, *Nonlinear Dynamics* 27 (2002) 69–85.
[28] A. Al Majid, R. Dufour, Harmonic response of a structure mounted on an isolator modelled with a hysteretic operator: experiments and prediction, *Journal of Sound and Vibration* 277 (1–2) (2004) 391–403.
[29] E. Bedrossian, S.O. Rice, The output properties of Volterra systems driven by Harmonic and Gaussian inputs, *Proceedings of the IEEE* 59 (12) (1971) 1688–1707.